

1 **Defining the Upper Nisyros Pumice (57.1 ± 1.5 ka) as new tephra isochrone for**
2 **linking early MIS-3 palaeoenvironmental records in the Aegean-Black Sea**
3 **gateway: new evidence from the Sea of Marmara**

4 Sabine Wulf^{1*}, M. Namık Çağatay², Oona Appelt³, K. Kadir Eriş², and Pierre Henry⁴

5 ¹ School of the Environment, Geography and Geosciences, University of Portsmouth, Lion
6 Terrace, Portsmouth, PO1 3HE, United Kingdom

7 ² İstanbul Technical University, EMCOL Research Centre and Department of Geological
8 Engineering, Ayazağa, 34469, İstanbul, Turkey

9 ³ Helmholtz Centre Potsdam, GFZ German Research Centre of Geosciences, Section 3.6,
10 Telegrafenberg, 14473 Potsdam, Germany

11 ⁴ CEREGE (UMR7330), Aix-Marseille Université, CNRS-IRD, 13330, Marseille 7, France

12 *Corresponding author: sabine.wulf@port.ac.uk (S. Wulf)

13
14 **Keywords:** Cryptotephra, Upper Nisyros Pumice, Sea of Marmara, Eastern Mediterranean

15 **Abstract**

16 The rhyolitic Upper Nisyros Pumice (UNP) from the Kos-Yali-Nisyros volcanic system has
17 been detected as a cryptotephra layer in lacustrine sediments from the Sea of Marmara (SoM).
18 A new independent age of the UNP eruption at 57.1 ± 1.5 cal ka BP has been interpolated
19 using a combination of radiocarbon dating, tephrochronology and wiggle-matching of the SoM
20 proxy record (Ca-curves) with Greenland oxygen isotope data, therewith confirming recently
21 published radioisotopic dates of UNP land deposits. The UNP tephra in the SoM was identified
22 by comparisons of the SoM tephra glass chemical dataset with published data of other marine
23 tephra records from the Aegean Sea and the Megali Limni lacustrine sediment sequence
24 (Lesvos Island). The stratigraphic position of the UNP tephra in these records verified its
25 deposition in the SoM at the onset of MIS-3 and specifically at the termination of Greenland
26 Interstadial GI-16. The new findings define the UNP tephra as a valuable time marker for the
27 synchronisation of palaeoenvironmental data for this time period and help spurring the

28 establishment of a robust tephrostratigraphical framework for the last ~70 kyr in the Aegean-
29 Black Sea region.

30 **1. Introduction**

31 Tephra layers in sedimentary records have been well established as tools for dating and
32 synchronizing palaeoclimate and -environmental data (e.g., Lowe, 2011), with numerous
33 examples derived from European records. Those include records from the Eastern
34 Mediterranean region which is characterised by intense and frequent explosive volcanic
35 activity (e.g., Italian and Aegean Arc volcanoes) and widespread tephra dispersal (e.g., Keller
36 et al., 1978; Narcisi and Vezzoli, 1999; Bourne et al., 2015; Satow et al., 2015; Giaccio et al.,
37 2012, 2019; Wulf et al., 2012, 2018, 2020; Vakhrameeva et al., 2018, 2019). To date,
38 numerous tephra markers from Italian volcanoes have been established as reliable isochrones
39 that provide precise and accurate absolute dates of the timing of their eruption (e.g., Giaccio
40 et al., 2012, 2017, 2019). However, dating of calc-alkaline tephras from Aegean Arc volcanoes
41 (e.g., Milos, Santorini, Kos, Nisyros, Yali) still lack absolute dating, mainly because advanced
42 radioisotopic dating techniques such as $^{40}\text{K}/^{40}\text{Ar}$ or $^{40}\text{Ar}/^{39}\text{Ar}$ are not suitable (e.g., Druitt et al.,
43 1999; Fabbro et al., 2013). One approach to overcome those dating problems is to interpolate
44 tephra deposition ages from sediment core chronologies of distal archives, as recently
45 demonstrated for Santorini tephra layers in Aegean Sea records (e.g., Satow et al., 2015,
46 2020; Wulf et al., 2020).

47 Compared to Santorini, the calc-alkaline Kos-Yali-Nisyros (KYN) magmatic system in the SE
48 part of the Aegean Sea still lacks a detailed tephrostratigraphy. Volcanic activity at the KYN
49 started approximately 3 Ma ago (Bachmann et al., 2010). One of the largest, caldera-forming
50 eruption occurred at 161.3 ± 1.1 ka resulting in the widespread dispersal of the Kos Plateau
51 Tuff (KPT; e.g., Smith et al., 1996; Hardiman, 1999; Allen, 2001). Subsequently, the volcanic
52 centres of Nisyros and Yali formed within the KPT caldera (Figs. 1a, c), which produced

53 several large explosive eruptions during the last 160 kyr (e.g., Pe-Piper and Moulton, 2008;
54 Bachmann et al., 2012).

55 Nisyros activities in particular were characterised by alternating effusive and explosive cycles
56 that erupted calc-alkaline basaltic-andesitic to rhyolitic lavas and pyroclastics (e.g., Di Paola,
57 1974; Limburg and Varekamp, 1991; Longchamp et al., 2011; Tomlinson et al., 2012a). Two
58 major Plinian, caldera-forming events, the Lower (LNP) and Upper Nisyros Pumice (UNP)
59 eruptions, formed massive tephra deposits on land and ash layers in distal terrestrial (Margari
60 et al., 2007) and marine (e.g., Vinci, 1985; Hardiman, 1999; Aksu et al., 2008) settings. The
61 timing of the LNP and UNP eruptions were controversially constrained to 110 - 28 ka (LNP;
62 Rehren, 1988; Barberi et al., 1988; Hardiman, 1999; Aksu et al., 2008) and >50 - 35 ka (UNP;
63 Vinci, 1985; Limburg and Varekamp, 1991; Margari et al., 2007; Karkanas et al., 2015),
64 prohibiting for a long time the use of these tephras as reliable isochrones. However, recent
65 advances in U-Th disequilibrium dating of zircon crystals have provided first absolute ages for
66 the LNP and UNP eruptions at 63.1 ± 4.7 ka and 58.4 ± 2.7 ka respectively (Popa et al., 2020);
67 those, however, still need verification by other independent dating techniques.

68 In this study, we report a cryptotephra in two sediment cores from the Sea of Marmara (SoM)
69 which connects the saline Aegean Sea and the brackish Black Sea basins via the Dardanelles
70 and Bosporus straits (Figs. 1a, b). We use a comprehensive tephra glass chemical dataset
71 and sediment accumulation rate age interpolation of the cryptotephra layer to establish a
72 robust correlation with and an independent age control for the UNP eruption. The new dataset
73 is used to re-evaluate previously published distal tephra findings in the Eastern Mediterranean
74 region, with special focus on Nisyros tephra findings in the Megali Limni lacustrine sequence
75 from Lesvos (Margari et al., 2007, 2009) and in Aegean Sea cores (Aksu et al., 2008; İşler et
76 al., 2016). We anticipate that the results will help to develop a more robust
77 tephrostratigraphical framework in the Aegean-Black Sea gateway region for the last 70 kyr.



80 **Figure 1:** a) Topographic map of the Eastern Mediterranean depicting the coring locations of
 81 MRS-CS18 and MRS-CS27 (blue stars) from the Sea of Marmara in relation to relevant
 82 volcanic provinces (red triangles) and other marine and terrestrial archives (blue dots) with
 83 Upper Nisyros Pumice occurrences. Tephra data are retrieved from Aksu et al. (2008) (MAR
 84 sites), Vinci (1985) (site MC27), Hardiman (1999) (purple site TRI172-26 with undefined
 85 Nisyros tephra occurrence), and Margari et al. (2007, 2009) (Megali Limni). White dots depict
 86 sites that lack Nisyros tephra (Tenaghi Philippon, Wulf et al., 2018; LC21, Satow et al., 2015;
 87 KL49, KL51, Wulf et al., 2020). The red dotted line indicates the proposed dispersal area of
 88 the UNP (this study). b) GoogleEarth inlet map showing the detailed positions of cores MRS-
 89 CS18 and MRS-C27 in the SoM (red dots). c) GoogleEarth inlet map of the Kos-Yali-Nisyros
 90 volcanic complex with the inferred KPT caldera (dotted yellow line).

91 2. Material and methods

92 Cores MRS-CS18 and MRS-CS27 used in this study were retrieved in 2015 on board of the
 93 RV Pourquoi pas? from 291 m below sea level (b.s.l.) and 313 m b.s.l. at the northeastern and
 94 western edges of the İmralı Basin in the SoM, respectively (Çağatay et al., 2019) (Fig. 1b).
 95 Sediments of both cores encompass alternating lacustrine and marine facies interrupted by a

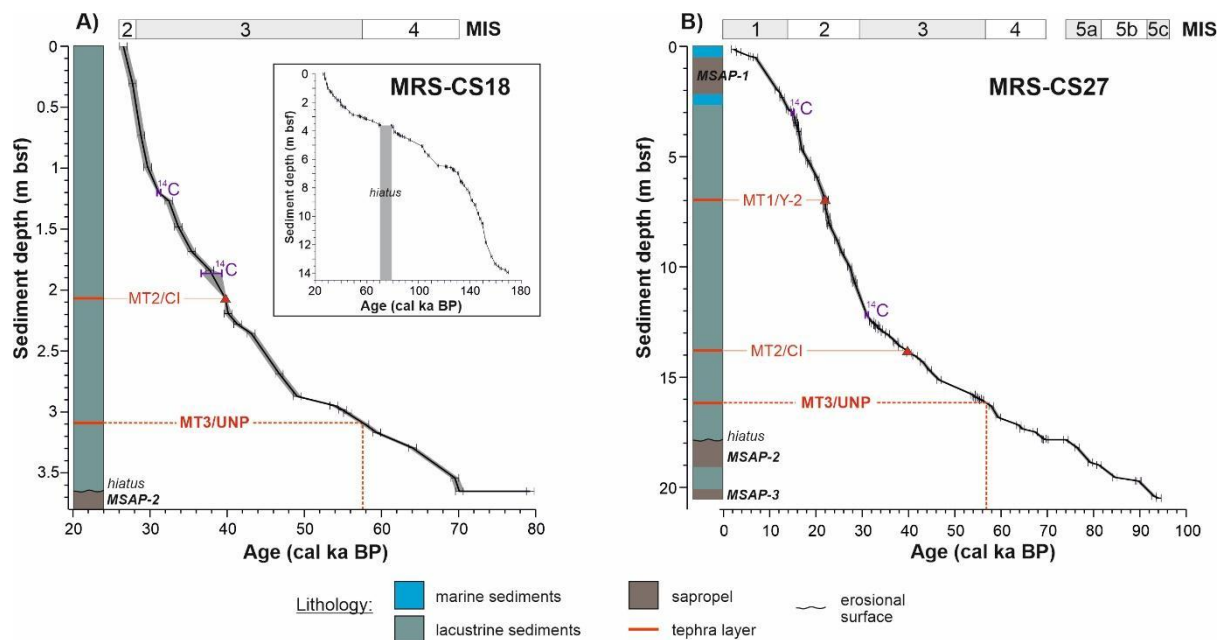
96 hiatus (Fig. 2) which indicates past major water level variations (Çağatay et al., 2019). Core
97 MRS-CS18 is a 14.05 m long sequence that contains an 8-cm-thick brown tephra layer (CS18-
98 MT2) at 2.03-2.11 mbsf and a 2-mm-thin ash layer (CS18-MT3) at 3.095 mbsf. Core MRS-
99 CS27 comprises a 20.45 m long sediment sequences that shows three distinct tephra layers:
100 the greyish CS27-MT1 (6.955-7.005 mbsf), the brownish CS27-MT2 (13.835-13.88 mbsf), and
101 the mm-thin CS27-MT3 ash layer at 16.18 mbsf. Based on their similar stratigraphic positions
102 and appearances in other SoM cores (Çağatay et al., 2015) the thick MT1 and MT2 tephra
103 layers have been tentatively correlated to the Y-2/Cape Riva eruption of Santorini and the Y-
104 5/Campanian Ignimbrite by Çağatay et al. (2019). The MT3 ash layer has been detected in
105 cores MRS-CS18 and MRS-CS27 by studying sections of increased values in magnetic
106 susceptibility and XRF-Calcium counts of sediments (Çağatay et al., 2009).

107 In this study, polished thin sections of tephra glass concentrate of the five tephra layers in
108 cores MRS-CS18 (MT2, MT3) and MRS-CS27 (MT1, MT2, MT3) were used to determine the
109 major element compositions of individual glass shards by electron probe microanalyses
110 (Supplement A). Measurements were carried out at the GFZ Potsdam (Germany) using a
111 JEOL-JXA8230 (WDS) probe with the following analytical setup: 15 kV accelerating voltage,
112 10 nA beam current and 8-10 µm beam size. Analytical count times were 20 seconds for the
113 elements Fe, Mn, Ti, Mg, P, and Cl, and 10 seconds for elements Si, Al, K, Ca, and Na
114 measured first. The natural Lipari obsidian (Hunt and Hill, 1996; Kuehn et al., 2011) and
115 artificial glass standards from the Max Planck Institute (MPI-glasses: ATHO-G, StHs6/80 and
116 GOR-132; Jochum et al., 2006) were used for data quality insurance (Supplement A).
117 Correlation of MT tephras used bivariate elemental plots of MT glass data and published glass
118 datasets (Fig. 3).

119 MT3 tephra ages in the SoM cores have been constrained by slightly revising the original age-
120 depth models of cores MRS-CS18 and MRS-CS27 (Çağatay et al., 2019), which are based
121 on a combination of wiggle-matching of the XRF-Ca-curves of both cores with interstadials of
122 the NGRIP oxygen isotope curve (Andersen et al., 2006; Svensson et al., 2008; Wolff et al.,

123 2010), radiocarbon dates on fossil shell samples, and tephrochronology (Fig. 2, Supplement
 124 A, Supplement Fig. B1). The revised sediment chronologies used the newest INTCAL20
 125 version by Reimer et al. (2020) for radiocarbon age calibration as well as up-to-date published
 126 tephra ages (Supplement Table B1). Tephra ages were calculated as average values from the
 127 2σ age ranges that were obtained by Bayesian modelling using the OxCal version 4.4.3 (Bronk
 128 Ramsey, 2021) (Supplement A). The revision of the original chronology of the Megali Limni
 129 lacustrine sequence ML01 (Margari et al., 2007, 2009) to estimate ages of potential Nisyros
 130 tephra equivalents used the same approach (see details in Supplement Fig. B2, Supplement
 131 C).

132



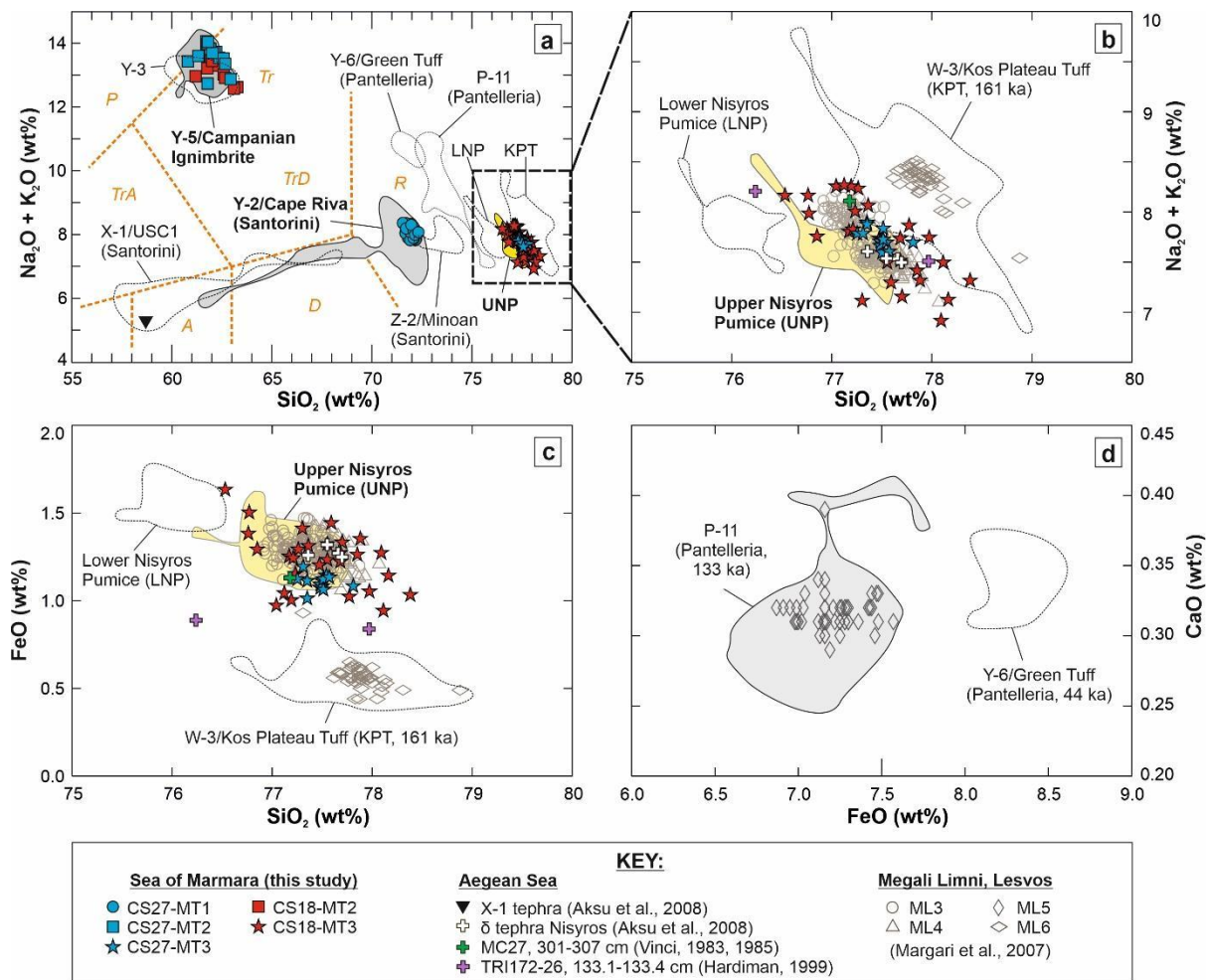
134
 135 **Figure 2:** Lithologies and age-depth models of Sea of Marmara cores MRS-CS18 (a) and
 136 MRS-CS27 (b) for the interval of the last 70 kyr. The inset graph (a) depicts the complete
 137 chronology of core MRS-CS18 as described in Çağatay et al. (2019). Core chronologies are
 138 based on a combination of radiocarbon dates (purple bars), imported tephra ages (red
 139 triangles) and wiggle-matching with the NGRIP oxygen isotope record (black bars). The
 140 MT3/UNP tephra ages (red dotted lines) derive from Bayesian modelling (Supplement A).
 141 MSAP represents typical sapropel layers in the Sea of Marmara, after marine re-connections
 142 during the interglacial periods.

143 **3. Results**

144 Tephras MT1 and MT2 in both SoM cores have rhyolitic and phono-trachytic major element
145 glass compositions that confirm the proposed correlation by Çağatay et al. (2019) to the Y-
146 2/Cape Riva and Y-5/Campanian Ignimbrite tephras, respectively (Fig. 3a, Supplement A).
147 Therefore, the published eruption ages for the Y-2 (22.02 ± 0.64 cal ka BP; Bronk Ramsey et
148 al., 2015) and Y-5 tephras (39.85 ± 0.14 $^{40}\text{Ar}/^{39}\text{Ar}$ ka, 39.78 ± 0.14 cal a BP; Giaccio et al.,
149 2017) were implemented as independent time markers for the construction of the revised age-
150 depth models (Fig. 2).

151 The glass composition of the MT3 cryptotephra layer is high-silica rhyolitic with concentration
152 ranges in SiO_2 of 76.5-78.4 wt%, Al_2O_3 of 11.9-12.6 wt%, FeO of 0.6-1.6 wt%, CaO of 0.7-1.2
153 wt%, K_2O of 3.6-4.9 wt%, and total alkalis ($\text{Na}_2\text{O}+\text{K}_2\text{O}$) of 7.1-8.3 wt% (normalised data)
154 (Supplement A). This major element glass chemistry is typical for tephras from the eastern
155 Aegean Arc and particularly from the Kos-Yali-Nisyros volcanic system. The MT3 glass
156 chemistry clearly matches the glass composition of the proximal deposits of the Upper Nisyros
157 Pumice (Tomlinson et al., 2012a), which can be well discriminated from the Lower Nisyros
158 Pumices (LNP) by slightly higher mean values in SiO_2 (77.2 vs. 76.1 wt%) and lower
159 concentrations in Al_2O_3 (12.3 vs. 12.9 wt%), FeO (1.3 vs. 1.5 wt%) and Na_2O (3.3 vs. 3.7 wt%)
160 (Figs. 3b-c).

161 The timing of the MT3 tephra deposition in the SoM has been interpolated by the revised age-
162 depth models of the MRS-CS18 and MRS-CS27 cores at $57,440 \pm 1570$ cal a BP and $56,710$
163 ± 1420 cal a BP, respectively (Fig. 2). The mean age yields at $57,080 \pm 1,500$ cal a BP, which
164 agrees well within its 2σ uncertainty with the U-Th disequilibrium (zircon) age of the proximal
165 Upper Nisyros Pumice deposits at 58.4 ± 2.7 ka BP obtained by Popa et al. (2020).
166 Furthermore, the chronostratigraphic position of the MT3 tephra as inferred from wiggle-
167 matching of the SoM Ca-curves with Greenland isotope data suggests a deposition in both
168 cores at the termination of Greenland Interstadial GI-16 (Fig. 4b-c).

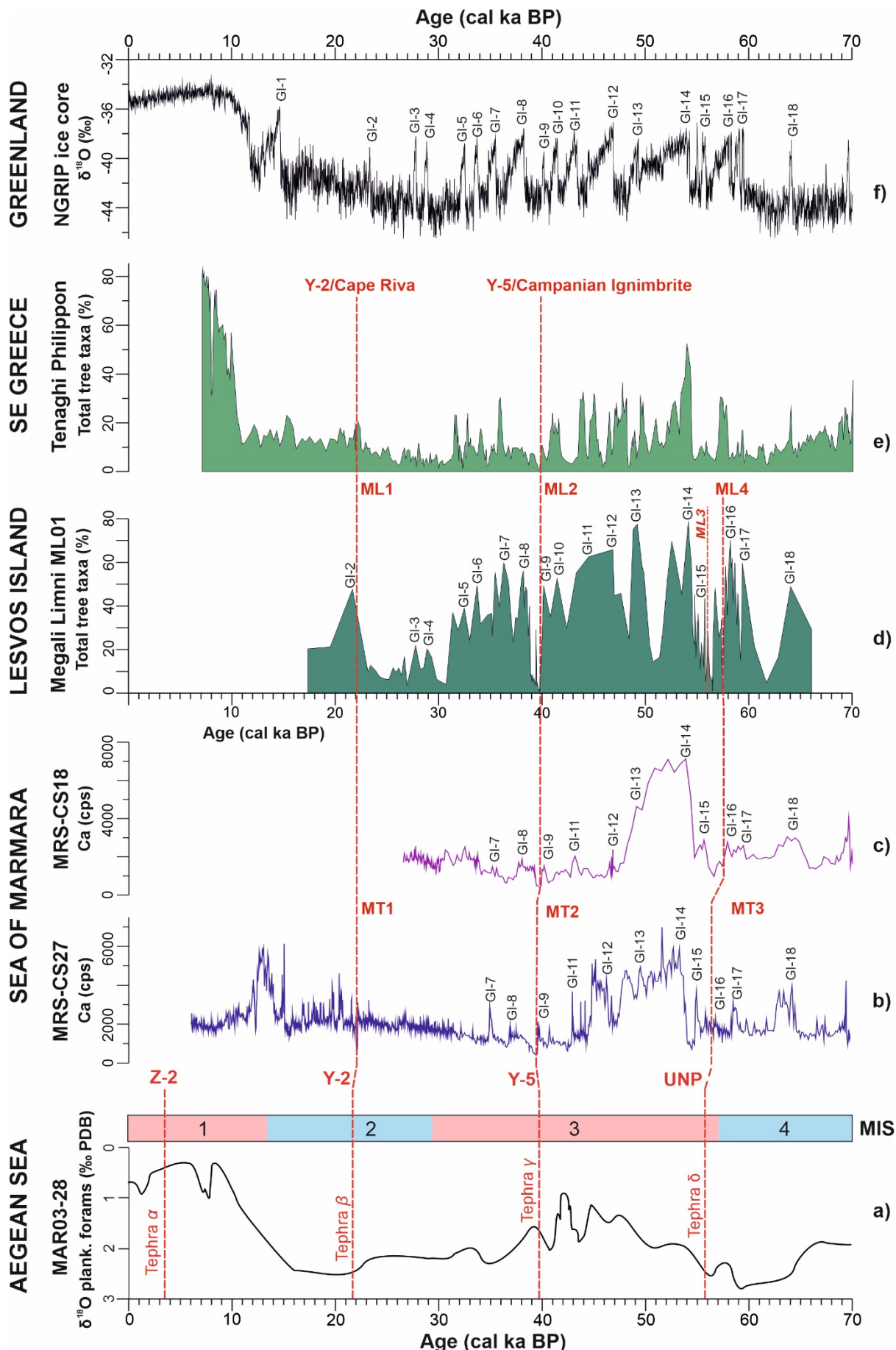


171 **Figure 3: (a-d)** Bivariate elemental plots of glass compositions of MT tephra of the Sea of
172 Marmara cores (this study), compared with published tephra datasets (envelopes) and
173 potential distal correlatives from the Aegean Sea (Aksu et al., 2008; Vinci, 1983, 1985;
174 Hardiman, 1999) and Megali Limni, Lesvos Island, Greece (Margari et al., 2007). Tephra glass
175 chemical datasets are retrieved from: Z-2/Minoan and Y-2/Cape Riva: Kwiecienska et al. (2008),
176 Tomlinson et al. (2015), Wulf et al. (2018, 2020); Y-3: Albert et al. (2015), Wulf et al. (2018,
177 2020); Y-5/Campanian Ignimbrite: Tomlinson et al. (2012b), Wulf et al. (2018); Y-6/Green Tuff:
178 Tomlinson et al. (2015); X-1/Upper Scoriae 1: Wulf et al. (2020); P-11: Satow et al. (2015),
179 Vogel et al. (2010), Leicher et al. (2016); Lower and Upper Nisyros Pumice (LNP, UNP):
180 Tomlinson et al. (2012a); W-3/Kos Plateau Tuff: Satow et al. (2015), Wegwerth et al. (2019),
181 Wulf et al. (2020).

182 **4. Discussion**

183 The MT3 tephra from the studied cores was previously correlated by Çağatay et al. (2019)
184 with the marine X-1 tephra based on its chronostratigraphic position below the Campanian
185 Ignimbrite and without verification by glass geochemical fingerprinting. The comparison with
186 distal tephra datasets shows that the MT3 tephra from the SoM correlates with the rhyolitic
187 tephra δ identified in several Aegean Sea cores (Aksu et al., 2008; İşler, 2012; İşler et al.,
188 2016), with a Nisyros tephra in southern Aegean Sea core MC27 (301-307 cm depth; Vinci,
189 1983, 1985), and with the ML3 and ML4 layers in the lacustrine core ML01 from Megali Limni,
190 Lesvos Island, Greece (Margari et al., 2007, 2009) (Figs. 3b-c). There is only a vague
191 compositional overlap with a proposed Lower Nisyros Pumice tephra in Adriatic Sea core
192 TRI172-26 (133.1-133.4 cm depth; Hardiman, 1999) (Figs. 3b-c), and the MT3 glass chemistry
193 is clearly distinct from the andesitic composition of the marine X-1 tephra in the Aegean Sea
194 (Fig. 3a).

195 Notably, the previous lack of glass chemical data of Nisyros tephra land deposits has for long
196 prevented reliable tephra correlations for the above-mentioned sites, and, in the case of Megali
197 Limni, partly confounded the core chronology and therewith the proxy data interpretations.
198 Hence, the respective tephra datasets of these records have been re-evaluated within this
199 study to allow for a direct comparison with SoM data (Fig. 4).



201 **Figure 4:** Comparison of palaeoenvironmental records of the last 70 kyr from the Aegean-
 202 Black Sea region by using mutual tephra isochrons (red dotted lines). **a)** Oxygen isotope curve
 203 of planktonic foraminifera from Aegean Sea core MAR03-28 (İşler et al., 2016) with timescale
 204 of Marine Isotope Stages (MIS); XRF-Ca-records of core MRS-CS27 (**b**) and MRS-CS18 (**c**)
 205 from the Sea of Marmara (Çağatay et al., 2019; this study) with positions of wiggle-matched
 206 Greenland Interstadials (GI). **d)** Total tree pollen percentages in the Megali Limni sequence,
 207 Lesvos Island (Margari et al., 2009; Sánchez Goñi et al., 2017) on a revised timescale (this
 208 study; see also Supplement Fig. B2-B4 and Supplement C) and with positions of wiggle-
 209 matched Gls. **e)** Total tree pollen percentages of the Tenaghi Philippon peat sequence,
 210 Southeast Greece (Müller et al., 2011; Wulf et al., 2018); **f)** Oxygen Isotope record of
 211 Greenland ice core NGRIP (NGRIP members, 2004) with positions of Greenland Interstadials
 212 (GI).

213

214 **4.1 Synchronisation with distal terrestrial tephra archives**

215 The comparison of the MT3 tephra data with the tephrostratigraphic record of the lacustrine
 216 record of Megali Limni (Margari et al., 2007, 2009; Pyle and Margari, 2009) is quite complex
 217 and requires a thorough revision of the published dataset. Margari et al. (2007, 2009) identified
 218 six visible tephra layers, namely ML1 to ML6, in core ML01 for which the age of the oldest
 219 tephra ML6 has been interpolated to ~57.6 cal ka BP. The sequence contains two closely-
 220 spaced Nisyros tephra layers, ML3 and ML4 (Margari et al., 2007), with identical glass
 221 composition that is also comparable to that of the UNP proximal deposits (Tomlinson et al.,
 222 2012a) and the SoM MT3 tephra (Fig. 3c-d). The deposition ages of the ML3 and ML4 tephra
 223 layers have been originally extrapolated to ~46.0 and ~46.8 cal ka BP (Margari et al., 2007;
 224 Pyle and Margari, 2009); those, however, are considerably younger than the UNP age
 225 constrained from the SoM sequences in this study.

226 The original age-depth model of the Megali Limni sequence is based on a combination of
 227 tephrochronology and radiocarbon dating (Margari et al., 2007). When reviewing the
 228 tephrochronological dataset, it is apparent that the youngest tephras ML1 and ML2, correlated
 229 by Margari et al. (2007) with the Y-2/Cape Riva and Y-5/Campanian Ignimbrite eruptions

230 respectively, are reliable time marker for the age-depth model. However, the two oldest
231 tephras ML5 and ML6 have been miscorrelated, and their imported ages therefore significantly
232 falsified the chronology. The younger ML5 tephra was previously correlated by Margari et al.
233 (2007) to the Y-6/Green Tuff of Pantelleria (44.1 ± 0.6 ka; Scaillet et al., 2013). However, FeO
234 values of ML5 tephra glasses are too low to justify an assignment to the Y-6 tephra but rather
235 suggest a correlation with the older Pantelleria P-11 tephra (133 ka; Satow et al., 2015) (Fig.
236 3d). A correlation with the P-11 tephra has been also postulated by Vogel et al. (2010) and is
237 strongly supported by the widespread dispersal of this tephra in the Balkan (e.g., Vogel et al.,
238 2010; Karkanas et al., 2015; Leicher et al., 2016) and southern Aegean Sea (Satow et al.,
239 2015) regions. The ML6 tephra, on the other hand, has been previously assigned to an
240 unknown Aegean Arc tephra (Margari et al., 2007) despite its glass composition showing an
241 unambiguous chemical match with the marine W-3 and the Kos Plateau Tuff (KPT; $161.3 \pm$
242 1.1 ka, Smith et al., 1996) (Fig. 3b-c). The stratigraphic position below the 133 ka-Pantelleria
243 tephra and the fact that the KPT is present in marine records from the Aegean-Black Sea
244 region (e.g., Satow et al., 2015; Wegwerth et al., 2019; Wulf et al., 2020) additionally support
245 a correlation of ML6 with the W-3/KPT eruption.

246 When considering the tephra ages of the revised ML5/P-11 and ML6/KPT correlations and re-
247 evaluating the Megali Limni pollen record of Margari et al. (2009) by wiggle-matching with the
248 Tenaghi Philippon pollen and the Greenland oxygen isotope records (Fig. 4d-f), it is evident
249 that the basal sediments of the Megali Limni core date back to the penultimate glacial instead
250 of MIS 4 (Supplement Figs. B2-B4, Supplement C). The new ML01 chronology also provides
251 revised modelled dates of the ML3 and ML4 tephras at $55,970 \pm 2040$ cal a BP and $57,490 \pm$
252 2030 cal a BP respectively (Fig. 4). The ML4 age at ~ 57.5 cal ka BP in particular agrees well
253 and within 2σ uncertainties with the UNP/MT3 extrapolated age in the SoM sediments (~ 57.1
254 cal ka BP) and with the U-Th disequilibrium zircon date of proximal UNP deposits at ~ 58.4 ka
255 by Popa et al. (2020). Furthermore, the ML4 tephra stratigraphic position in the Megali Limni
256 pollen record confirms the occurrence of the UNP eruption at the termination of Greenland

257 Interstadial GI-16 (Fig. 4, Supplement Figs. B3-B4). The revised chronostratigraphic
258 information in combination with the lack of proximal and marine distal evidence for more than
259 one UNP eruption suggest that ML4 is most likely the primary tephra layer in the Megali Limni
260 sequence and that the younger ML3 tephra layer might have been derived from reworking
261 processes which, however, needs to be further investigated.

262

263 ***4.2 Links with marine tephra archives and UNP dispersal***

264 The majority of Nisyros tephra findings derives from the marine realm. For example, Aksu et
265 al. (2008) identified the thin ‘tephra δ’ layer in several sediment cores collected from across
266 the Aegean Sea and north of Nisyros volcano (MAR-sites in Fig. 1a). Tephra δ is
267 stratigraphically positioned between the Campanian Ignimbrite tephra layer and sapropel S3
268 and has been dated by extrapolation of the marine oxygen isotope stratigraphy to originally
269 42-44 ka BP (Aksu et al., 2008). Higher-resolution $\delta^{18}\text{O}$ records published by İşler et al. (2016)
270 have corrected this age to 53-58 ka BP, therewith placing tephra δ at the onset of MIS 3 (Fig.
271 4a). A previous correlation of tephra δ with the Lower Nisyros Pumice by Aksu et al. (2008)
272 has been revised to the Upper Nisyros pumices by Tomlinson et al. (2012a), and the new SoM
273 MT3 dataset corroborates this assignment (Figs. 3b-c). Therewith, the UNP tephra, together
274 with the Campanian Ignimbrite and the Santorini Y-2, presents an additional valuable
275 isochrone for the glacial period that allows for detailed palaeoceanographic reconstructions of
276 the Aegean-Black Sea gateway region (Fig. 4).

277 Other UNP tephra findings in the Aegean Sea include a 6-cm-thick layer in core MC27,
278 located ~120 km south of Nisyros (Vinci, 1983, 1985). The chronostratigraphic position of the
279 MC27 tephra is only poorly constrained, hence impeding a direct comparison with the SoM
280 and other Aegean Sea data. Nevertheless, the MC27 tephra plays an important role for
281 reconstruction of the UNP tephra dispersal in the Aegean Sea region since its occurrence
282 indicates an additional southerly dispersion alongside the predominant northerly dispersal

283 pattern as evidenced from the MAR Aegean Sea, Megali Limni, and SoM cores. However,
284 MC27 is to date the only distal core south of Nisyros containing the UNP tephra, while other
285 nearby high-resolution tephra archives, i.e. cores LC21 (Satow et al., 2015), KL49 and KL51
286 (Wulf et al., 2020) lack this tephra (Fig. 1a). Therefore, further investigations are required to
287 demonstrate the primary character of the MC27 tephra prior to interpreting this complex
288 dispersal pattern.

289

290 **5. Conclusions**

291 The new findings of the Upper Nisyros Pumice as MT3 tephra in the Sea of Marmara in
292 combination with high-resolution proxy datasets provided a new modelled age of the UNP
293 eruption at 57.1 ± 1.5 cal ka BP. This tephra age confirms the radioisotopic date of the UNP
294 by Popa et al. (2020) and agrees well with the revised modelled age of the UNP distal tephra
295 equivalent ML4 in the Megali Limni terrestrial record. The stratigraphic position of the UNP in
296 palaeoenvironmental records of the Aegean-Black Sea region suggests its deposition at the
297 termination of Greenland Interstadial GI-16 (SoM, Megali Limni) and at the onset of MIS 3
298 (Aegean Sea cores).

299 The occurrence of the UNP tephra in the SoM represents to date the furthest finding
300 in the north-eastern part of the Aegean-Black Sea region, suggesting likely a transport by
301 strong prevailing southerly winds at the time of the eruption and implying the possibility to
302 detect this tephra in even more distal positions than previously believed. It is therefore
303 recommended that future palaeoenvironmental studies in this region implement detailed
304 (crypto)tephra studies to take advantage of this new tephra isochrone.

305

306 Acknowledgements

307 We thank the scientific team of Marsite cruise and the captains and crews of RV Pourquoi
308 pas? for the recovery of cores MRS-CS18 and MRS-CS2. The Marsite cruise was co-funded
309 by the EC FP7 project MARSITE (grant number: 308417), the “Laboratoire d'Excellence”
310 LabexMER (ANR-10-LABX-19) through the projects called Micro-GaMa and MISS Marmara,
311 and by a grant from the French government under the program “Investissements d'Avenir”.
312 We also thank Mehmet Ali Oral of Geological Engineering Department at ITU, for the
313 preparation of polished thin sections for tephra EPM analysis.

314

315 References

- 316 Aksu, A.E., Jenner, G., Hiscott, R.N., Isler, E.B., 2008. Occurrence, stratigraphy and
317 geochemistry of Late Quaternary tephra layers in the Aegean Sea and the Marmara Sea.
318 Mar. Geol. 252, 174-192. <https://doi.org/10.1016/j.margeo.2008.04.004>
- 319 Albert, P.G., Hardiman, M., Keller, J., Tomlinson, E.L., Smith, V.C., Bourne, A.J., Wulf, S.,
320 Zanchetta, G., Sulpizio, R., Müller, U.C., Pross, J., Ottolini, L., Matthews, I.P., Blockley,
321 S.P.E., Menzies, M.A., 2015. Revisiting the Y-3 tephostratigraphic marker: a new
322 diagnostic glass geochemistry, age estimate, and details on its climatostratigraphical
323 context. Quat. Sci. Rev. 118, 105-121. <https://doi.org/10.1016/j.quascirev.2014.04.002>
- 324 Allen, S.R., 2001. Reconstruction of a major caldera-forming eruption from pyroclastic
325 deposit characteristics: Kos Plateau Tuff, eastern Aegean Sea. J. Volcanol. Geoth. Res.
326 105, 141-162. [https://doi.org/10.1016/S0377-0273\(00\)00222-5](https://doi.org/10.1016/S0377-0273(00)00222-5)
- 327 Andersen, K.K., Svensson, A., Johnsen, S., S.O. Rasmussen, S.O., Bigler,
328 M., Rothlisberger, R., Ruth, U., Siggaard-Andersen, M.L., Steffensen, J.P., Dahl-
329 Jensen, D., Vinther, B.M., Clausen, H.B., 2006. The Greenland ice core chronology 2005,
330 15–42 ka. part 1: constructing the time scale. Quat. Sci. Rev. 25, 3246-3257.
331 <https://doi.org/10.1016/j.quascirev.2006.08.002>
- 332 Bachmann, O., Schoene, B., Schnyder, C., Spikings, R., 2010. $^{40}\text{Ar}/^{39}\text{Ar}$ and U/Pb dating of
333 young rhyolites in the Kos-Nisyros volcanic complex, Eastern Aegean Arc (Greece): age
334 discordance due to excess ^{40}Ar in biotite. Geochem. Geophy. Geosy. 11, Q0AA08.
335 <https://doi.org/10.1029/2010GC003073>

- 336 Bachmann, O., Deering, C.D., Ruprecht, J.S., Huber, C., Skopelitis, A., Schnyder, C., 2012.
337 Evolution of silicic magmas in the Kos-Nisyros volcanic center, Greece: a petrological
338 cycle associated with caldera collapse. *Contrib. Mineral. Petr.* 163, 151-166.
339 <https://doi.org/10.1007/s00410-011-0663-y>
- 340 Barberi, F., Navarro, J.M., Rosi, M., Santacroce, R., Sbrana, A., 1988. Explosive interaction
341 of magma with groundwater: insights from xenoliths and geothermal drillings. *Rend. Soc.*
342 *Ital. Mineral. Petrol.* 43, 901–926. <http://hdl.handle.net/11568/15177>
- 343 Bourne, A.J., Albert, P.G., Matthews, I.P., Trincardi, F., Wulf, S., Asioli, A., Blockley, S.P.E.,
344 Keller, J., Lowe, J.J., 2015. Tephrochronology of core PRAD 1-2 from the Adriatic Sea:
345 insights into Italian explosive volcanism for the period 200-80 ka. *Quat. Sci. Rev.* 116, 28-
346 43. <https://doi.org/10.1016/j.quascirev.2015.03.006>
- 347 Bronk Ramsey, C., 2021. OxCal version 4.4.3. <https://c14.arch.ox.ac.uk/oxcal.html>.
- 348 Bronk Ramsey, C., Albert, P.G., Blockley, S.P.E., Hardiman, M., Housley, R.A., Lane, C.S.,
349 Lee, S., Matthews, I.P., Smith, V.C., Lowe, J.J., 2015. Improved age estimates for key
350 Late Quaternary European tephra horizons in the RESET lattice. *Quat. Sci. Rev.* 118, 18-
351 32. <https://doi.org/10.1016/j.quascirev.2014.11.007>
- 352 Çağatay, M.N., Eriş, K.K., Ryan, W.B.F., Sancar, Ü., Polonia, A., Akçer, S., Biltekin, D.,
353 Gasperini, L., Görür, N., Lericolais, G., Bard, E., 2009. Late Pleistocene-
354 Holocene evolution of the northern shelf of the Sea of Marmara. *Mar. Geol.* 265, 87-100.
355 <https://doi.org/10.1016/j.margeo.2009.06.011>
- 356 Çağatay, M.N., Wulf, S., Sancar, Ü., Özmaral, A., Vidal, L., Henry, P., Appelt, O., Gasperini,
357 L., 2015. The tephra record from the Sea of Marmara for the last ca. 70 ka and its
358 palaeoceanographic implications. *Mar. Geol.* 361, 96-110.
359 <https://doi.org/10.1016/j.margeo.2015.01.005>
- 360 Çağatay, M.N., Eriş, K.K., Makaroğlu, Ö., Yakupoğlu, N., Henry, P., Leroy, S.A.G., Uçarkuş,
361 G., Sakınç, M., Yalamaz, B., Bozyigit, C., Kende, J., 2019. The Sea of Marmara during
362 Marine Isotope Stages 5 and 6. *Quat. Sci. Rev.* 220, 124-141.
363 <https://doi.org/10.1016/j.quascirev.2019.07.031>
- 364 Di Paola, G.M., 1974. Volcanology and petrology of Nisyros Island (Dodecanese, Greece). *B.*
365 *Volcanol.* 38, 944-987. <https://doi.org/10.1007/BF02597100>
- 366 Druitt, T.H., Edwards, L., Mellors, R.M., Pyle, D.M., Sparks, R.S.J., Lanphere, M., Davies,
367 M., Barriero, B., 1999. Santorini Volcano. *Geol. Soc. Spec. Publ.* 19, 165 pp.
- 368 Fabbro, G.N., Druitt, T.H., Scaillet, S., 2013. Evolution of the crustal magma plumbing
369 system during the build-up to the 22-ka caldera-forming eruption of Santorini (Greece). *B.*
370 *Volcanol.* 75, 767. <https://doi.org/10.1007/s00445-013-0767-5>
- 371 Giaccio, B., Nomade, S., Wulf, S., Isaia, R., Sottili, G., Cavuoto, G., Galli, P., Messina, P.,
372 Sposato, A., Sulpizio, R., Zanchetta, G., 2012. The late MIS 5 Mediterranean tephra

- 373 markers: a reappraisal from peninsular Italy terrestrial records. Quat. Sci. Rev. 56, 31-45.
374 <https://doi.org/10.1016/j.quascirev.2012.09.009>
- 375 Giaccio, B., Hajdas, I., Isaia, R., Deino, A., Nomade, S., 2017. High-precision ^{14}C and $^{40}\text{Ar}/^{39}\text{Ar}$
376 dating of the Campanian Ignimbrite (Y-5) reconciles the time-scale of climatic cultural
377 processes at 40 ka. Sci. Rep. 7, 45940. <https://doi.org/10.1038/srep45940>
- 378 Giaccio, B., Leicher, N., Mannella, G., Monaco, L., Regattieri, E., Wagner, B., Zanchetta, G.,
379 Gaeta, M., Marra, F., Nomade, S., Palladino, D.M., Pereira, A., Scheidt, S., Sottili, G.,
380 Wonik, T., Wulf, S., Zeeden, C., Aristegui, D., Cavinato, G.P., Dean, J.R., Florindo, F.,
381 Leng, M., Macrì, P., Niespolo, E., Renne, P.R., Rolf, C., Sadori, L., Thomas, C., Tzedakis,
382 P.C., 2019. Extending the tephra and palaeoenvironmental record of the Central
383 Mediterranean back to 430 ka: a new core from Fucino Basin, central Italy. Quat. Sci.
384 Rev. 225, 106003. <https://doi.org/10.1016/j.quascirev.2019.106003>
- 385 Hardiman, J.C., 1999. Deep sea tephra from Nisyros Island, eastern Aegean Sea, Greece.
386 Geol. Soc. Spec. Publ. 161, 69–88. <https://doi.org/10.1144/GSL.SP.1999.161.01.06>
- 387 Hunt, J.B., Hill, P.G., 1996. An inter-laboratory comparison of the electron probe
388 microanalysis of glass geochemistry. Quatern. Int. 34-36, 229-241.
389 [https://doi.org/10.1016/1040-6182\(95\)00088-7](https://doi.org/10.1016/1040-6182(95)00088-7)
- 390 İşler, E.B., 2012. Paleoceanographic and paleoclimatic evolution of the Aegean Sea since
391 the last Interglacial (~130 ka BP) with special emphasis on sapropel formation. PhD
392 Thesis, Memorial University of Newfoundland.
393 <http://research.library.mun.ca/id/eprint/12114>
- 394 İşler, E.B., Hiscott, R.N., Aksu, A.E., 2016. Late Quaternary chronostratigraphy of the
395 Aegean Sea sediments: special reference to the ages of sapropels S1-S5. Turk. J. Earth
396 Sci. 25, 1-18. <https://doi.org/10.3906/yer-1501-37>
- 397 Jochum, K.P., Stoll, B., Herwig, K., Willbold, M., Hofmann, A.W., et al., 2006. MPI-DING
398 reference glasses for in situ microanalysis: New reference values for element
399 concentrations and isotope ratios. Geochem. Geophys. Geosy. 7(2), Q02008.
400 <https://doi.org/10.1029/2005GC001060>
- 401 Karkanas, P., White, D., Lane, C.S., Stringer, C., Davies, W., Cullen, V.L., Smith, V.C.,
402 Ntinou, M., Tsartsidou, G., Kyparissi-Apostolika, N., 2015. Tephra correlations and
403 climatic events between the MIS6/5 transition and the beginning of MIS3 in Theopetra
404 Cave, central Greece. Quat. Sci. Rev. 118, 170–181.
405 <https://doi.org/10.1016/j.quascirev.2014.05.027>
- 406 Keller, J., Ryan, W.B.F., Ninkovich, D., Altherr, R., 1978. Explosive volcanic activity in the
407 Mediterranean over the past 200,000 yr as recorded in deep-sea sediments. Geol. Soc.
408 Am. Bull. 89, 591-604. [https://doi.org/10.1130/0016-7606\(1978\)89%3C591:EVAITM%3E2.0.CO;2](https://doi.org/10.1130/0016-7606(1978)89%3C591:EVAITM%3E2.0.CO;2)

- 410 Kuehn, S.C., Froese, D.G., Shane, P.A.R., INTAV Intercomparison Participants, 2011. The
411 INTAV intercomparison of electron-beam microanalysis of glass by tephrochronology
412 laboratories: Results and recommendations. *Quatern. Int.* 246, 19-47.
413 <https://doi.org/10.1016/j.quaint.2011.08.022>
- 414 Kwiecien, O., Arz, H.W., Lamy, F., Wulf, S., Bahr, A., Röhl, U., Haug, G.H., 2008. Estimated
415 reservoir ages of the Black Sea since the last glacial. *Radiocarbon* 50(1), 99-118.
416 <https://doi.org/10.1017/S0033822200043393>
- 417 Leicher, N., Zanchetta, G., Sulpizio, R., Giacco, B., Wagner, B., Nomade, S., Francke, A.,
418 Del Carlo, P., 2016. First tephrostratigraphic results of the DEEP site record from Lake
419 Ohrid (Macedonia and Albania). *Biogeosciences* 13, 2151-2178.
420 <https://doi.org/10.5194/bg-13-2151-2016>
- 421 Limburg, E.M., Varekamp, J.C., 1991. Young pumice deposits on Nisyros, Greece. *B.*
422 *Volcanol.* 54(1), 68–77. <https://doi.org/10.1007/BF00278207>
- 423 Longchamp, C., Bonadonna, C., Bachmann, O., Skopelitis, A., 2011. Characterization of
424 tephra deposits with limited exposure: the example of the two largest explosive eruptions
425 at Nisyros volcano (Greece). *B. Volcanol.* 73, 1337-1352. <https://doi.org/10.1007/s00445-011-0469-9>
- 427 Lowe, D.J., 2011. Tephrochronology and its application: A review. *Quat. Geochronol.* 6, 107-
428 153. <https://doi.org/10.1016/j.quageo.2010.08.003>
- 429 Margari, V., Pyle, D.M., Bryant, C., Gibbard, P.L., 2007. Mediterranean tephra stratigraphy
430 revisited: Results from a long terrestrial sequence on Lesvos Island, Greece. *J. Volcanol.*
431 *Geoth. Res.* 163, 34-54. <https://doi.org/10.1016/j.jvolgeores.2007.02.002>
- 432 Margari, V., Gibbard, P.L., Bryant, C.L., Tzedakis, P.C., 2009. Character of vegetational and
433 environmental changes in southern Europe during the last glacial period; evidence from
434 Lesvos Island, Greece. *Quat. Sci. Rev.* 28, 1317-1339.
435 <https://doi.org/10.1016/j.quascirev.2009.01.008>
- 436 Martin-Puertas, C., Brauer, A., Wulf, S., Ott, F., Lauterbach, S., Dulski, P., 2014. Annual
437 proxy data from Lago Grande di Monticchio (southern Italy) between 76 and 112 ka: new
438 chronological constraints and insights on abrupt climatic oscillations. *Clim. Past* 10, 2099-
439 2114. <https://doi.org/10.5194/cp-10-2099-2014>
- 440 Milner, A.M., Roucoux, K.H., Collier, R.E.L., Müller, U.C., Pross, J., Tzedakis, P.C., 2016.
441 Vegetation responses to abrupt climatic changes during the Last Interglacial Complex
442 (Marine Isotope Stage 5) at Tenaghi Philippon, NE Greece. *Quat. Sci. Rev.* 154, 169-181.
443 <https://doi.org/10.1016/j.quascirev.2016.10.016>
- 444 Müller, U.C., Pross, J., Tzedakis, P.C., Gamble, C., Kotthoff, U., Schmiedl, G., Wulf, S.,
445 Christianis, K., 2011. The role of climate in the spread of modern humans into Europe.
446 *Quat. Sci. Rev.* 30, 273-279. <https://doi.org/10.1016/j.quascirev.2010.11.016>

- 447 Narcisi, B., Vezzoli, L., 1999. Quaternary stratigraphy of distal tephra layers in the
448 Mediterranean - an overview. *Global Planet. Change* 21, 31-50.
449 [https://doi.org/10.1016/S0921-8181\(99\)00006-5](https://doi.org/10.1016/S0921-8181(99)00006-5)
- 450 NGRIP members, 2004. High-resolution record of Northern Hemisphere climate extending
451 into the last interglacial period. *Nature* 431, 147-151. <https://doi.org/10.1038/nature02805>
- 452 Pe-Piper, G., Moulton, B., 2008. Magma evolution in the Pliocene-Pleistocene succession of
453 Kos, South Aegean arc (Greece). *Lithos* 106(1–2), 110–124.
454 <https://doi.org/10.1016/j.lithos.2008.07.002>
- 455 Popa, R.-G., Guillong, M., Bachmann, O., Szymanowski, D., Ellis, B., 2020. U-Th zircon
456 dating reveals a correlation between eruptive styles and repose periods at the Nisyros-
457 Yali volcanic area, Greece. *Chem. Geol.* 555, 11930.
458 <https://doi.org/10.1016/j.chemgeo.2020.119830>
- 459 Pyle, D.M., Margari, V., 2009. Reply: Correlation of a widespread Pleistocene tephra marker
460 from the Nisyros-Yali volcanic complex, Greece. *J. Volcanol. Geoth. Res.* 181, 251-254.
461 <https://doi.org/10.1016/j.jvolgeores.2008.11.033>
- 462 Rehren, T., 1988. Geochemie und Petrologie von Nisyros (Ostliche Agais). PhD thesis,
463 University of Freiburg, pp. 167.
- 464 Reimer, P.J., Austin, W.E.N., Bard, E., Bayliss, A., Blackwell, P.G., Bronk Ramsey, C.,
465 Butzin, M., Cheng, H., Edwards, R.L., Friedrich, M., Grootes, P.M., Guilderson, T.P.,
466 Hajdas, I., Heaton, T.J., Hogg, A.G., Hughen, K.A., Kromer, B., Manning, S.W.,
467 Muscheler, R., Palmer, J.G., Pearson, C., van der Plicht, J., Reimer, R.W., Richards,
468 D.A., Scott, E.M., Southon, J.R., Turney, C.S. M., Wacker, L., Adolphi, F., Büntgen, U.,
469 Capano, M., Fahrni, S.M., Fogtmann-Schulz, A., Friedrich, R., Köhler, P., Kudsk, S.,
470 Miyake, F., Olsen, J., Reinig, F., Sakamoto, M., Sookdeo, A., Talamo, S., 2020. The
471 IntCal20 Northern Hemisphere Radiocarbon Age Calibration Curve (0–55 cal kBP).
472 *Radiocarbon* 62(4), 725–757. <https://doi.org/10.1017/RDC.2020.41>
- 473 Sánchez Goñi, M.F., Desprat, S., Daniau, A.-L., Bassinot, F.C., Polanco-Martínez, J.M.,
474 Harrison, S.P., Allen, J.R.M., Anderson, R.S., Behling, H., Bonnefille, R., Burjachs, F.,
475 Carrión, J.S., Cheddadi, R., Clark, J.S., Combouieu-Nebout, N., Courtney-Mustaphi,
476 C.J., Debusk, G.H., Dupont, L.M., Finch, J.M., Fletcher, W.J., Giardini, M., González, C.,
477 Gosling, W.D., Grigg, L.D., Grimm, E.C., Hayashi, R., Helmens, K., Heusser, L.E., Hill, T.,
478 Hope, G., Huntley, B., Igarashi, Y., Irino, T., Jacobs, B., Jiménez-Moreno, G., Kawai, S.,
479 Kershaw, P., Kumon, F., Lawson, I.T., Ledru, M.-P., Lezine, A.-M., Liew, P.M., Magri, D.,
480 Marchant, R., Margari, V., Mayle, F.E., McKenzie, M., Moss, P., Müller, S., Müller, U.C.,
481 Naughton, F., Newnham, R.M., Oba, T., Pérez-Obiol, R., Pini, R., Ravazzi, C., Roucoux,
482 K.H., Rucina, S.M., Scott, L., Takahara, H., Tzedakis, P.C., Urrego, D.H., van Geel, B.,
483 Valencia, B.G., Vandergoes, M.J., Vincens, A., Whitlock, C.L., Willard, D.A., Yamamoto,

- 484 M., 2017. The ACER pollen and charcoal database: a global resource to document
485 vegetation and fire response to abrupt climate changes during the last glacial period.
486 *Earth Syst. Sci. Data* 9 (2), 679-695. <https://doi.org/10.5194/essd-2017-4>.
- 487 Satow, C., Tomlinson, E.L., Grant, K.M., Albert, P.G., Smith, V.C., Manning, C.J., Ottolini, L.,
488 Wulf, S., Rohling, E.J., Lowe, J.J., Blockley, S.P.E., Menzies, M.A., 2015. A new
489 contribution to the Late Quaternary tephrostratigraphy of the Mediterranean: Aegean Sea
490 core LC21. *Quat. Sci. Rev.* 117, 96-112. <https://doi.org/10.1016/j.quascirev.2015.04.005>
- 491 Satow, C., Grant, K., Wulf, S., Schulz, H., Mallon, A., Matthews, I., Lowe, J., 2020. Detection
492 and characterisation of Eemian marine tephra layers within the sapropel S5 sediments of
493 the Aegean and Levantine Seas. *Quaternary* 3(1), 6. <https://doi.org/10.3390/quat3010006>
- 494 Scaillet, S., Vita-Scaillet, G., Rotolo, S.G., 2013. Millennial-scale phase relationships
495 between ice-core and Mediterranean marine records: insights from high-precision
496 $^{40}\text{Ar}/^{39}\text{Ar}$ dating of the Green Tuff of Pantelleria, Sicily Strait. *Quat. Sci. Rev.* 78, 141-154.
497 <https://doi.org/10.1016/j.quascirev.2013.08.008>
- 498 Smith, P.E., York, D., Chen, Y., Evensen, N.M., 1996. Single crystal $^{40}\text{Ar}-^{39}\text{Ar}$ dating of a
499 Late Quaternary paroxysm on Kos, Greece: Concordance of terrestrial and marine ages.
500 *Geophys. Res. Lett.* 23, 3047-3050. <https://doi.org/10.1029/96GL02759>
- 501 Svensson, A., Andersen, K.K., Bigler, M., Clausen, H.B., Dahl-Jensen, D., Davies, S.M.,
502 Johnsen, S.J., Muscheler, R., Rasmussen, S.O., Röhlisberger, R., Steffensen, J.P.,
503 Vinther, B.M., 2006. The Greenland Ice Core Chronology 2005, 15-42 ka. Part 2:
504 comparison to other records. *Quat. Sci. Rev.* 25, 3258-3267.
505 <https://doi.org/10.1016/j.quascirev.2006.08.003>
- 506 Svensson, A., Andersen, K.K., Bigler, M., Clausen, H.B., Dahl-Jensen, D., Davies, S.M.,
507 Johnsen, S.J., Muscheler, R., Parrenin, F., Rasmussen, S.O., Röhlisberger, R.,
508 Seierstad, I., Steffensen, J.P., Vinther, B.M., 2008. A 60000-year Greenland stratigraphic
509 ice core chronology. *Clim. Past* 4, 47-57. <https://doi.org/10.5194/cp-4-47-2008>
- 510 Tomlinson, E.L., Kinzig, H.S., Smith, V.C., Blundy, J.D., Gottsmann, J., Müller, W., Menzies,
511 M.A., 2012a. The Upper and Lower Nisyros Pumices: revisions to the Mediterranean
512 tephrostratigraphic record based on micron-beam glass geochemistry. *J. Volcanol.*
513 *Geoth. Res.* 243-244, 69–80. <https://doi.org/10.1016/j.jvolgeores.2012.07.004>
- 514 Tomlinson, E.L., Arienzo, I., Civetta, L., Wulf, S., Smith, V.C., Hardiman, M., Lane, C.S.,
515 Carandente, A., Orsi, G., Rosi, M., Muller, W., Menzies, M.A., 2012b. Geochemistry of the
516 Phlegraean Fields (Italy) proximal sources for major Mediterranean tephras: Implications
517 for the dispersal of Plinian and co-ignimbritic components of explosive eruptions.
518 *Geochim. Cosmochim. Ac.* 93, 102-128. <https://doi.org/10.1016/j.gca.2012.05.043>
- 519 Tomlinson, E.L., Smith, V.C., Albert, P.G., Aydar, E., Civetta, L., Cioni, R., Çubukçu, E.,
520 Gertisser, R., Isaia, R., Menzies, M.A., Orsi, G., Rosi, M., Zanchetta, G., 2015. The major

- 521 and trace element glass compositions of the productive Mediterranean volcanic sources:
522 tools for correlating distal tephra layers in and around Europe. Quat. Sci. Rev. 118, 48-66.
523 <https://doi.org/10.1016/j.quascirev.2014.10.028>
- 524 Vakhrameeva, P., Koutsodendris, A., Wulf, S., Fletcher, W.J., Appelt, O., Knipping, M.,
525 Gertisser, R., Trieloff, M., Pross, J., 2018. The cryptotephra record of the Marine Isotope
526 Stage 12 to 10 interval (460-335 ka) at Tenaghi Philippon, Greece: Exploring
527 chronological markers for the Middle Pleistocene of the Mediterranean region. Quat. Sci.
528 Rev. 200, 313–333. <https://doi.org/10.1016/j.quascirev.2018.09.019>
- 529 Vakhrameeva, P., Wulf, S., Koutsodendris, A., Tjallingii, R., Fletcher, W.J., Appelt, O.,
530 Ludwig, T., Knipping, M., Trieloff, M., Pross, J., 2019. Eastern Mediterranean volcanism
531 during Marine Isotope Stages 9 to 7e (335–235 ka): Insights based on cryptotephra
532 layers at Tenaghi Philippon, Greece. J. Volcanol. Geoth. Res. 380, 31–47.
533 <https://doi.org/10.1016/j.jvolgeores.2019.05.016>
- 534 Vinci, A., 1983. A new ash layer ‘Nisyros Layer’ in the Aegean Sea sediments. Bollettino di
535 Oceanologia Teorica ed Applicata 1, 341–342.
- 536 Vinci, A., 1985. Distribution and chemical composition of tephra layers from Eastern
537 Mediterranean abyssal sediments. Mar. Geol. 64, 143–155. [https://doi.org/10.1016/0025-3227\(85\)90165-3](https://doi.org/10.1016/0025-3227(85)90165-3)
- 539 Vogel, H., Wagner, B., Zanchetta, G., Sulpizio, R., Rosén, P., 2010. A Paleoclimate record
540 with tephrochronological age control for the last glacial-interglacial cycle from lake Ohrid,
541 Albania and Macedonia. J. Paleolimnol. 44, 295–310. <https://doi.org/10.1007/s10933-009-9404-x>
- 543 Wegwerth, A., Dellwig, O., Wulf, S., Plessen, B., Kleinhanns, I.C., Nowaczyk, N.C., Jiabo, L.,
544 Arz, H.W., 2019. Major hydrological shifts in the Black Sea “Lake” in response to ice
545 sheet collapses during MIS 6 (130–184 ka BP). Quat. Sci. Rev. 219, 126–144.
546 <https://doi.org/10.1016/j.quascirev.2019.07.008>
- 547 Wolff, E.W., Chappellaz, J., Blunier, T., Rasmussen, S.O., Svensson, A., 2010. Millennial-
548 scale variability during the last glacial: The ice core record. Quat. Sci. Rev. 29, 2828–
549 2838. <https://doi.org/10.1016/j.quascirev.2009.10.013>
- 550 Wulf, S., Keller, J., Paterne, M., Mingram, J., Lauterbach, S., Opitz, S., Sottili, G., Giaccio,
551 B., Albert, P.G., Satow, C., Tomlinson, E.L., Viccaro, M., Brauer, A., 2012. The 100–133
552 ka record of Italian explosive volcanism and revised tephrochronology of Lago Grande di
553 Monticchio. Quat. Sci. Rev. 58, 104–123. <https://doi.org/10.1016/j.quascirev.2012.10.020>
- 554 Wulf, S., Hardiman, M., Staff, R.A., Koutsodendris, A., Appelt, O., Blockley, S.P.E., Lowe,
555 J.J., Manning, C.J., Ottolini, L., Schmitt, A.K., Smith, V.C., Tomlinson,
556 E.L., Vakhrameeva, P., Knipping, M., Kotthoff, U., Milner, A.M., Müller, U.C., Christianis,
557 K., Kalaitzidis, S., Tzedakis, C., Schmiedl, G., Pross, J., 2018. The Marine Isotope Stage

558 1 to 5 cryptotephra record of Tenaghi Philippon, Greece: Towards a detailed
559 tephrostratigraphic framework for the Eastern Mediterranean region. Quat. Sci. Rev. 186,
560 236-262. <https://doi.org/10.1016/j.quascirev.2018.03.011>

561 Wulf, S., Keller, J., Satow, C., Gertisser, R., Kraml, M., Grant, K.M., Appelt, O.,
562 Vakhrameeva, P., Koutsodendris, A., Hardiman, M., Schulz, H., Pross, J.,
563 2020. Advancing Santorini's tephrostratigraphy: new glass geochemical data and
564 improved marine-terrestrial tephra correlations for the past ~360 kyrs. Earth-Sci.
565 Rev. 200, 102964. <https://doi.org/10.1016/j.earscirev.2019.102964>

566

567 **Supplement A:** EPMA glass data of tephra layers MT-1, MT-2 and MT-3 from cores MRS-
568 CS18 and MRS-CS27; EPMA glass reference data for data control; Bayesian age models of
569 cores MRS-CS18 and MRS-CS27.

570 **Supplement Table B1:** Revised age constraints (radiocarbon, tephra) of Sea of Marmara
571 sediment cores MRS-CS18 and MRS-CS27.

572 **Supplement Figure B1:** OxCal age-depth models of cores MRS-CS18 and MRS-CS27.

573 **Supplement Figure B2:** Comparison of original and revised age-depth models of Megali
574 Limni core ML01.

575 **Supplement Figure B3:** Selected pollen taxa (Total tree taxa, Juniper + Pinus, and Artemisia)
576 of the ML01 sequence from Megali Limni on a depth scale.

577 **Supplement Figure B4:** Selected pollen taxa (Total tree taxa, Juniper + Pinus, and Artemisia)
578 of the ML01 sequence from Megali Limni on a revised time scale (this study).

579 **Supplement C:** Revised age constraints and Bayesian age model of Megali Limni core
580 ML01 (this study); ML01 pollen dataset from Margari et al. (2009) and Sánchez Goñi et al.
581 (2017) on a revised timescale; Age constraints used for the original ML01 chronology of
582 Margari et al. (2007, 2009).